Earth, Planets and Space

FULL PAPER Open Access

Simulated east–west differences in F-region peak electron density at Far East mid-latitude region

Zhipeng Ren[1,2,3,4*], Biqiang Zhao[1,2,3,4], Weixing Wan[1,2,3,4], Libo Liu[1,2,3,4], Xing Li[5,6] and Tingting Yu[1,2,3,4]

Abstract

Using TIME3D-IGGCAS model, we simulated the east–west differences in F-region peak electron density (NmF2) in the Far East mid-latitude region near the longitudinal sectors with very clear zonal variations of geomagnetic declination, and mainly analyzed the influence of the geomagnetic field configuration on the east–west differences. We found that, after removing the longitudinal variations of neutral parameters, TIME3D-IGGCAS can better represent the observed relative east–west difference (R_{ew}) features. R_{ew} is mainly negative (West NmF2 > East NmF2) at noon and positive (East NmF2 > West NmF2) at evening–night. The magnitude of daytime negative R_{ew} is weaker in winter and stronger in summer, and the daytime R_{ew} shows two negative peaks around two equinoxes. With the increasing solar flux level, the magnitude of R_{ew} mainly becomes larger, and the two daytime negative peaks slightly shift to June Solstice. With the decreasing geographical latitude, R_{ew} mainly becomes positive, and the two daytime negative peaks slightly shift to June Solstice. Our simulation also suggested that the thermospheric zonal wind plays an important role in the formation of the ionospheric east–west differences in the Far East mid-latitude region. The observed solar activity dependency of the ionospheric EW differences may be driven primarily by corresponding zonal wind changes with solar activity, whereas the observed latitudinal dependency of the differences is associated with primarily zonal wind and secondarily meridional wind latitudinal variations.

Keywords: Ionospheric east–west difference, Ionospheric longitudinal variation, Ionospheric region anomalies, Mid-latitude ionosphere, Ionosphere–thermosphere coupling

Introduction

The ionospheric spatial structure is an important essential question in the ionospheric research, and has been studied for several decades. The ionospheric parameters vary with altitude, latitude and longitude, and researchers had paid close attention to the ionospheric longitudinal variability in recent years. Many mechanisms can cause the ionospheric longitudinal variability. For example, through the coupling between the ionosphere and atmosphere below, the non-migrating tide can affect the ionospheric longitudinal variability, and play a key role in the formation of ionospheric longitudinal structures. Numerous observational and simulated evidences suggested that the DE3 tide is one of the main sources of the ionospheric and thermospheric longitudinal wavenumber-4 structure (e.g., Ren et al. 2008, 2009a, 2010, 2011a, 2012a, 2014; Wan et al. 2008, 2010, 2012). However, the geomagnetic fields play an important role in the ionospheric longitudinal variability, and cause a series of ionospheric regional anomalies (e.g., Ren et al. 2009b, 2012b, c).

The ionospheric regional anomalies, e.g., Weddell Sea Anomaly, can cause longitudinal difference between the anomalous region and the other longitude sectors, and can also be regarded as a kind of ionospheric longitude structures. Since 1957, researchers had found that the

*Correspondence: zpren@mail.iggcas.ac.cn
[1] Key Laboratory of Earth and Planetary Physics, Institute of Geology and Geophysics, Chinese Academy of Sciences, Beijing 100029, People's Republic of China
Full list of author information is available at the end of the article

maximum in foF2 diurnal variation in local summer around the Weddell Sea occurs at night, and this unusual nighttime enhancement has been called the "Weddell Sea Anomaly" (WSA) (e.g., Bellchambers and Piggott 1958; Dudeney and Piggot 1978). Similar diurnal variations have also been found in other ionospheric density parameters (e.g., TEC) (e.g., Chang et al. 2015; Klimenko et al. 2015; Lean et al. 2016; Richards et al. 2017). Because a similar anomaly in electron density can also be found in other region (such as the East Asian region), this kind of ionospheric anomalous are now called Mid-latitude Summer Nighttime Anomaly (MSNA) (e.g., He et al. 2009; Thampi et al. 2009; Chen et al. 2016; Richards et al. 2014, 2018). Liu et al. (2010) and Ren et al. (2012b) pointed out that MSNA mainly occur in three regions, the South Pacific region, the Northern Atlantic region, and the East Asian region. MSNA phenomenon causes obvious longitudinal difference between above three regions and their adjacent regions.

Based on the ground-based GPS total electron content (TEC) observations, Zhang et al. (2011) found obvious TEC east–west (EW) differences in mid-latitude region of the continental US. They found that the phase of EW difference depends on the local time. Meanwhile, using the ground observations of ionosondes and space-based measurements, Zhao et al. (2013) also found obvious EW differences in the mid-latitude F-region peak electron density (NmF2) in the Far East middle latitude region. Previous research suggested that the mechanism of EW difference may be similar to that of MSNA phenomena over East Asian and Northern Atlantic. Since MSNA and EW difference occur at the middle latitudes, the influence of high-latitude ionospheric convection and the longer summer sunlight hours are unlikely to be the main mechanism of these phenomena (see Penndorf 1965; Kohl and King 1967; Horvath and Essex 2003). Because the geomagnetic field declinations of the regions where MSNA and EW difference exist change clearly as a function of longitude, the geomagnetic field configuration may greatly affect the formation of these phenomena. Researches supported that the thermospheric winds play important roles in MSNA (e.g., Lin et al. 2009; Liu et al. 2010; Chen et al. 2011; Ren et al. 2012b; Thampi et al. 2011; Wang et al. 2015). Expressly, Ren et al. (2012b) and Liu et al. (2010) pointed out that MSNA mainly occur in the regions where the geomagnetic field declinations are larger. Zhao et al. (2013) and Zhang et al. (2011) both show that the phase of the ionospheric East–West difference depends on the local time, and suggested that it is caused by the coupling of diurnal variation of thermospheric zonal wind and the longitudinal variation of magnetic declination over the Far East regions and US. As evidence, Zhang et al. (2012a) has shown a good linear relationship between the plasma density EW differential and the nighttime thermospheric eastward wind over Millstone Hill. However, as suggested by Zhang et al. (2012b), the EW difference is actually different from MSNA phenomenon. First, MSNA is an increase in ionospheric plasma density at night relative to its daytime levels, while the EW differences show obvious diurnal variations. Second, the EW differences occur in all seasons, while MSNA mainly occurs near local summer. However, the mechanisms of the amplitude of EW difference changing with season and solar activity are still not clear.

In the ionospheric researches, especially in the study of the mechanism of ionospheric variability, simulations play important roles. In recent years, researchers have done much work in modeling the thermosphere/ionosphere system, and a series of ionospheric/thermospheric models, such as TIEGCM and GITM, have been widely used to study the ionospheric longitude structures and regional anomalies. Coupled ionosphere–thermosphere models can well simulate the influence of ionosphere–thermosphere coupling on the ionospheric regional anomalies. However, such models have some limitations in studying the impact of the thermosphere. For example, because the thermospheric parameters are self-consistent with the ionospheric parameters, it is difficult for coupled ionosphere–thermosphere models to change the thermosphere artificially in simulation, and the ionospheric model is more flexible to simulate the thermospheric effects in some conditions. Here, we will simulate the EW differences in ionospheric NmF2 at the Far East mid-latitude region in realistic geomagnetic fields with the TIME3D-IGGCAS model (an ionospheric model), compare the simulation results with the observations, and analyze the physical mechanism controlling the climatology of the local EW difference.

TIME3D-IGGCAS model and inputs

Historically, any F2 layer behaviors departure from the solar zenith angle dependence as predicted by the Chapman ionization theory has been called an "anomaly". The ionospheric regional anomalies often connect with the geomagnetic anomaly area, and the non-dipole components of geomagnetic fields normally control these geomagnetic anomalies. However, the geomagnetic field in many theoretical ionospheric models (e.g., SAMI3) has been taken simply as a dipole field. Although dipole field is a good low- and mid-latitudes geomagnetic field approximation, it could not describe the regional anomalies of geomagnetic fields. Thus, we need simulate ionospheric behaviors with realistic geomagnetic fields. Some theoretical models (e.g., TIEGCM) adopt realistic magnetic fields, but they are based on geographic

coordinates, which need to obtain the top boundary condition from the empirical models. In this condition, the top boundary will affect the simulation results.

Ren et al. (2012d) had developed a three-dimensional theoretical ionospheric model, referred to as the Three-Dimensional Theoretical Ionospheric Model of the Earth at Institute of Geology and Geophysics, Chinese Academy of Sciences (TIME3D-IGGCAS). This model adopts a magnetic APEX coordinates system, so it is possible to simulate the ionospheric behaviors in realistic geomagnetic fields or in the other non-dipole geomagnetic fields. TIME3D-IGGCAS is based on the geomagnetic tubes, and needs no top boundary conditions. This model was first developed as a mid- and low-latitude three-dimensional ionospheric model. Recently, we developed a new high-latitude ionosphere module, and extended this model to a real global model. Now, this model covers the whole ionosphere and plasmasphere (the height range between 130 km and 22,000 km). Through solving the equations of mass continuity, motion and energy, the self-consistently time-dependent three-dimensional structures of the main ionospheric and plasmaspheric parameters can be obtained, including number densities, temperature and velocity vectors of ion (O^+, H^+, He^+, NO^+, $O_2{}^+$, $N_2{}^+$) and electrons. There are 24 magnetic meridional planes in TIME3D-IGGCAS, and every plane includes about 57 magnetic field lines. The horizontal resolution is about 15° in magnetic longitude. In the low-latitude, mid-latitude and high-latitude region, the horizontal resolutions in magnetic latitude, respectively, are about 1°, 4°, and 2°. The principal input parameters, such as the neutral winds, temperature, densities, and $\mathbf{E} \times \mathbf{B}$ drifts, mainly are from empirical models or observations. This model can reproduce well the main features of the global ionosphere, and some details of this model can be found in Ren et al. (2012d).

Results and discussion

To study the ionospheric east–west asymmetry, we simulate ionospheric diurnal variations for different months. These simulations are mainly performed for medium solar activity and geomagnetic quiet conditions, corresponding to a $F_{10.7}$ index of 140 and an *A*p index of 4. The initial conditions of the temperature and number densities of ion and electron are from IRI model, and the thermospheric empirical models, such as NRLMSIS-00 and HWM-93, provide the neutral temperature, densities and horizontal winds. Richmond empirical model, which mainly provides quiet-day F-region $\mathbf{E} \times \mathbf{B}$ drifts for low solar activity conditions, determines the meridional and zonal $\mathbf{E} \times \mathbf{B}$ drifts (Richmond et al. 1980). Previous researches suggested that the middle latitude F-region ionosphere is mainly controlled by thermospheric neutral winds (see also Liu et al. 2003). Because this work focuses on the middle latitude EW differences in ionospheric F-region plasma density at Far East mid-latitude region, we still can use Richmond model in our simulation. To obtain the presented results, 3 model day runs, whose time steps are 300 s, were made.

The ionosphere changes with the geomagnetic latitude and the geographic latitude. At Far East mid-latitude region, the geographic latitude is approximately parallel to the geomagnetic latitude. Hence, by comparing two Far East mid-latitude stations of the same geographic latitude, it can effectively avoid the interference of the geographical and geomagnetic latitude variation and of geomagnetic latitude variation, and focus on the influence of east–west asymmetry. In the following, similar to Zhao et al. (2013), we mainly compare ionosphere parameters at two Far East mid-latitude stations with the same geographic latitude. The ionospheric E–W difference may vary with longitudinal difference of the stations. To compare with the observations at Wakkanai and Almaata reported by Zhao et al. (2013), we mainly analyze the simulated seasonal and diurnal variations of NmF2 at 45° N 75° E (geomagnetic declination: − 8°) and at 45° N 142.5° E (geomagnetic declination: 3.7°).

Figure 1a, b, respectively, shows the simulated seasonal and diurnal variations of NmF2 at 45° N 75° E ($NmF2_{West}$) and at 45° N 142.5° E ($NmF2_{East}$) (case I), which are in units of 10^{11} electron/m^3. As shown in Fig. 1a, at 45° N 75° E, although the NmF2 mainly shows an annual variation in the evening, the daytime NmF2 shows a semi-annual variation. In all seasons, NmF2 maximizes near 1100LT, and MSNA does not occur. This agrees with normal ionospheric diurnal variations of the Chapman ionization theory. However, different diurnal variations of NmF2 can be found at 45° N 142.5° E. The mean NmF2 at 45° N 142.5° E is mainly smaller than that at 45° N 75° E. Although NmF2 still shows a diurnal variation and maximizes near 1200 LT near December Solstice, NmF2 maximizes near 1900LT in June Solstice. The sunset NmF2 is about 100% larger than that at noon in June Solstice, and the higher nighttime NmF2 lasts for about 3 h near sunset. This is a typical MSNA case, and similar phenomenon in the Far East region is also found by Liu et al. (2010). As shown in Fig. 1b, the NmF2 maximum shifts toward later local times in the first half year, and shifts back to earlier local times in the latter half of the year, and there is a second NmF2 peak near sunrise between April and July. The simulated seasonal and diurnal variations agree with those observed by Zhao et al. (2013). We show ΔNmF2 ($NmF2_{east}$–$NmF2_{west}$) in Fig. 1c, and the white lines in this figure represent the zero lines. As shown in Fig. 1c, ΔNmF2 shows obvious annual variations at all local times, and ΔNmF2 mainly decreases from local winter

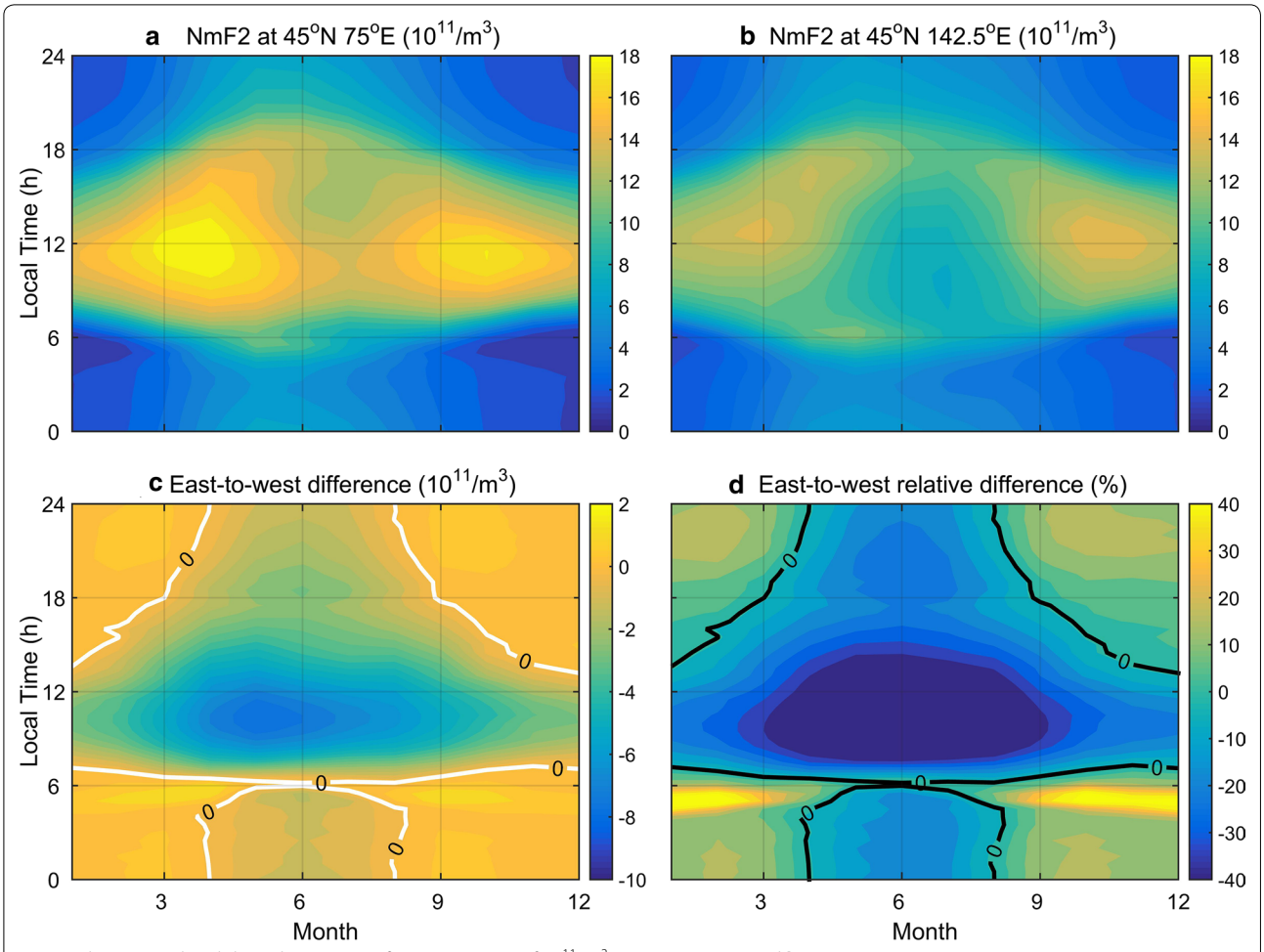

Fig. 1 The seasonal and diurnal variations of NmF2 (in units of 10^{11}/m^3) **a** at 45° N 75° E and **b** at 45° N 142.5° E, **c** ΔNmF2 ($NmF2_{east}$-$NmF2_{west}$, in units of 10^{11}/m^3), and **d** relative differences (R_{ew}, in units of %). The solid lines in these plots represent the zero lines

to local summer. Similar to Zhao et al. (2013) and Zhang et al. (2011), we also use R_{ew} index to analyze the relative EW difference, where $R_{ew} = (NmF2_{east} - NmF2_{west})/(NmF2_{east} + NmF2_{west}) \times 200\%$. As shown in Fig. 1d, the seasonal and diurnal variations of R_{ew} are similar to that of ΔNmF2, but R_{ew} minimizes around June. However, this seasonal and diurnal variation shows some different features with those observed by Zhao et al. (2013). First, the observed daytime negative R_{ew} exhibits two minimum peaks around May and June, while the simulated R_{ew} minimizes around June. Second, the observed R_{ew} is positive at evening–night, while the simulated R_{ew} shows negative values at local summer evening.

Because the neutral parameters from empirical models vary with longitude, both geomagnetic fields and longitudinal variations of neutral parameters may cause the above ionospheric EW differences. Hence, after removing the longitudinal variations of neutral parameters (e.g., neutral temperature, neutral density, neutral composition, and neutral winds), we simulate the seasonal and diurnal variations of NmF2 with the global longitudinal averaged neutral parameters (case II), and show them in Fig. 2. Because of the change of the neutral parameters, there are some differences in NmF2 in two cases at 45° N 75° E. However, the seasonal and diurnal variations of NmF2 at 45° N 142.5° E in case I and in case II agree with each other well. The MSNA, which is weaker than that at 45° N 142.5° E, also occurs at 45° N 75° E. The ΔNmF2 in case II, as shown in Fig. 2c, also shows some different features. First, the ionospheric EW differences in case II is weak than that in case I. Second, ΔNmF2 shows obvious semi-annual variations in most of local time. Third, ΔNmF2 in case II is mainly positive at evening–night, while ΔNmF2 in case I shows negative value at local summer evening. Figure 2d shows the seasonal and diurnal variations of R_{ew} in case II, and three features can be found. First, R_{ew} is mainly negative at noon and positive at evening–night. Second, the magnitude of daytime

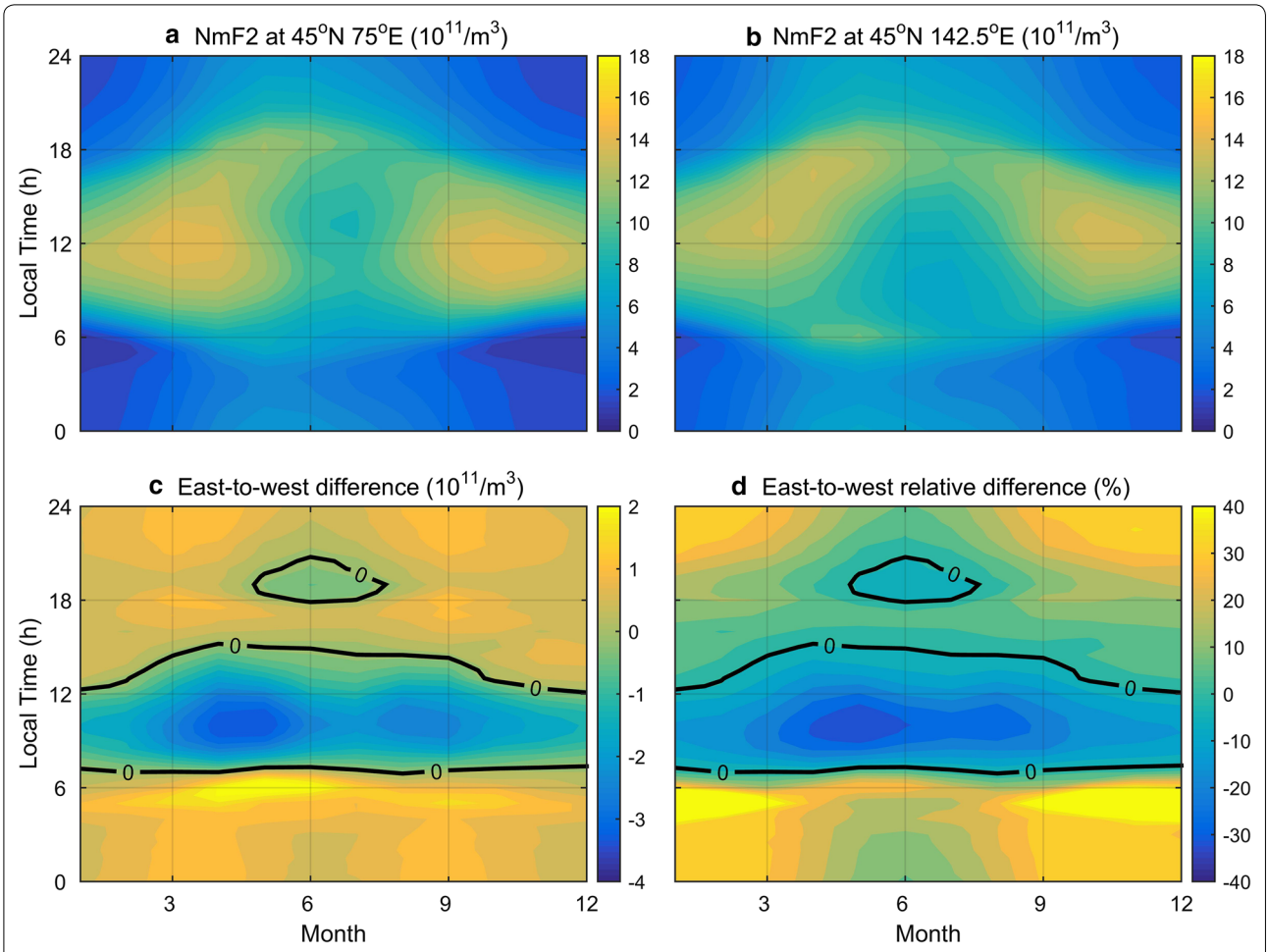

Fig. 2 Same as Fig. 1, but for case II, which removes the longitudinal variations of neutral parameters

negative R_{ew} is weaker in winter and stronger in summer, and the daytime R_{ew} shows two negative peaks at May and at August. Third, the nighttime R_{ew} shows obviously annual variations. Compared with the R_{ew} observed by Zhao et al. (2013), although the third feature disappears in observation, the first two features agree well with the observations. The third feature may be mainly caused by MSNA occurring in the East Asian region, and Ren et al. (2012b) suggested that MSNA in the East Asian region is mainly driven by the thermospheric meridional wind (see Ren et al. 2012b and its references). Not only the seasonal and diurnal variations, but also the magnitude of R_{ew} agrees well with that observed by Zhao et al. (2013). Because we remove the neutral parameters' longitudinal variations, the simulated NmF2 EW differences may be mainly driven by the longitudinally uniformly distributed zonal winds whose effects depend on the longitudinal variations of geomagnetic fields.

The following problem is the source of the ionospheric EW differences in the Far East mid-latitude region. Zhao et al. (2013) pointed out that the Far East region shows obvious east–west gradient in geomagnetic declination, and the geomagnetic fields may play a pivotal role in the EW differences. The geomagnetic fields can affect the ionosphere through at least two ways. First, the magnetic fields can control the ionospheric dynamo and affect the ionospheric electrodynamic drifts and distribution of the plasma density in the ionosphere and plasmasphere (e.g., Ren et al. 2009b, 2011b, 2012c). Second, the geomagnetic field modifies the direction and velocity of the plasma field-aligned diffusion, which are driven by plasma pressure gradient, by the neutral winds, and by gravity. In the middle latitude region, the second mechanism is more important. Zhao et al. (2013) suggested that the thermospheric zonal wind plays an important role in the ionospheric EW differences in the East-Asia region. However, Ren et al. (2012b) had found that the influence of thermospheric meridional wind on the ionospheric diurnal variation (or MSNA) at Far East mid-latitude region is obviously stronger than the impact of zonal

wind. Thus, we simulate the contributions of different components of thermospheric wind on the formation of the ionospheric EW differences. We simulate ionospheric seasonal and diurnal variations for medium solar flux level in four conditions: (case a) with both zonal and meridional winds; (case b) only with zonal wind; (case c) only with meridional wind; (case d) without any winds. Similar to case II, the longitudinal variations of neutral parameters are removed in these simulations. Figure 3 shows the seasonal and diurnal variations of R_{ew} in four cases, and the black solid lines represent the zero lines. As shown in Fig. 3, the magnitude of R_{ew} driven by all thermospheric winds together (Fig. 3a) and by zonal wind (Fig. 3b) is obviously larger than that driven by meridional wind (Fig. 3c) and without thermospheric wind (Fig. 3d). The seasonal and diurnal variations of R_{ew} in case b show three features. First, R_{ew} is mainly negative at noon and positive at evening–night. Second, R_{ew} mainly shows annual variations in most of local time. Third, although there are some differences, a semi-annual variation also can be found in morning R_{ew}. However, in most of local times and seasons, R_{ew} in case b agrees with that in case a. Hence, the coupling between the geomagnetic field configuration and thermospheric zonal winds plays a pivotal role in the formation of the ionospheric EW differences at Far East mid-latitude region. Although the influence is weak, the meridional wind also can drive the ionospheric EW differences at Far East mid-latitude area. However, the diurnal variation of R_{ew} driven by meridional winds (Fig. 3c), which is negative at afternoon–evening section and positive at other local time, is obviously different from that driven by zonal winds (Fig. 3b). This result suggests that meridional winds modulate the diurnal variation of R_{ew}. For example, although the June evening minimum driven by zonal winds appear near 0300LT (case b), the June evening minimum driven by all thermospheric winds appear near 2000LT (case a). We should notice that a weak semi-annual variation can also be found in morning R_{ew} driven by meridional winds. The daytime double minima (or the daytime semi-annual

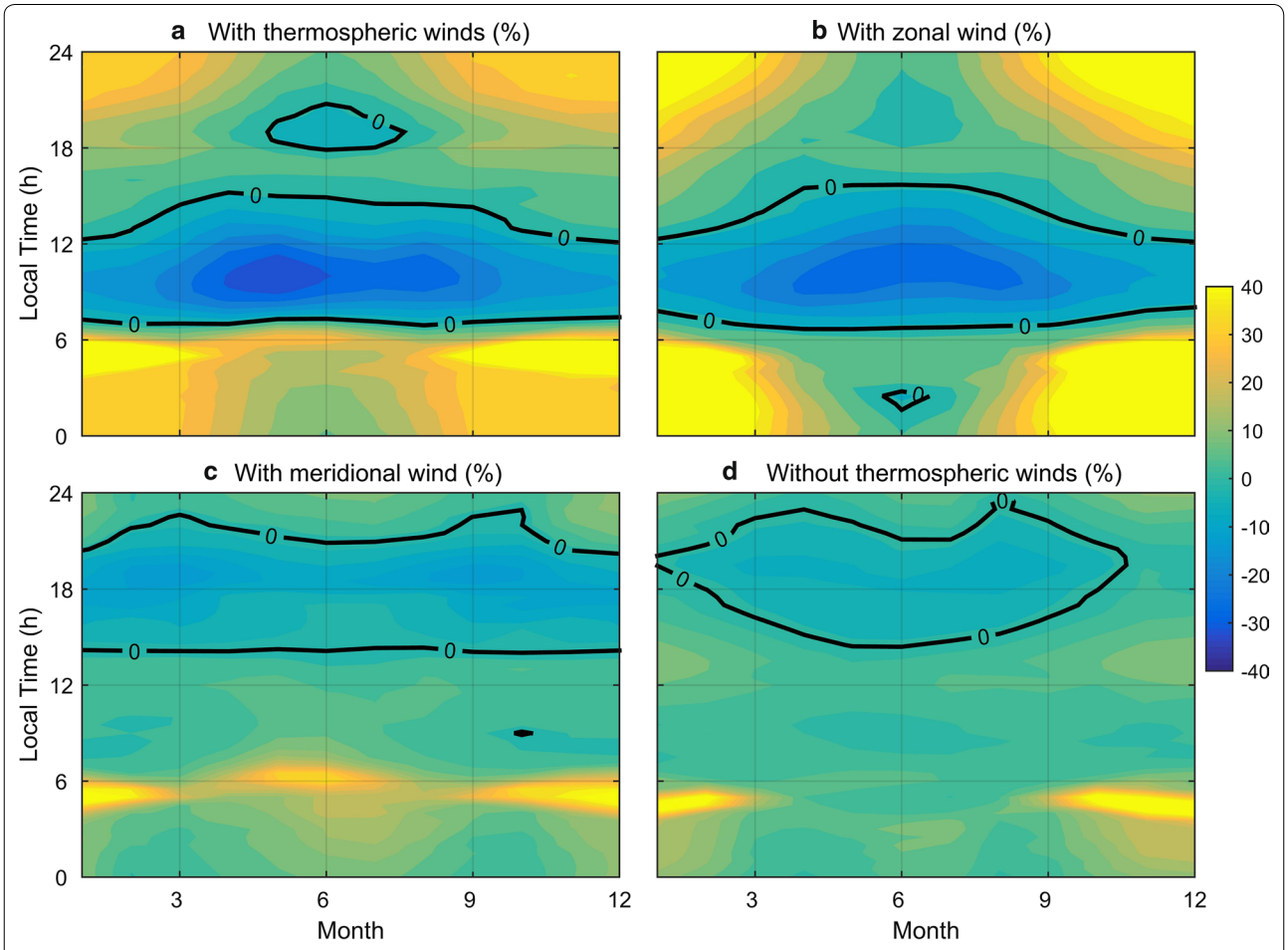

Fig. 3 The seasonal and diurnal variations of R_{ew} (in units of %) driven **a** by all thermospheric winds, **b** by thermospheric zonal wind, **c** by thermospheric meridional wind, and **d** no thermospheric winds

variation) is an important feature of the ionospheric east–west differences in the Far East mid-latitude region (Zhao et al. 2013). Our simulations suggested that this phenomenon is driven by the combination of meridional and zonal winds, and the zonal wind plays a more important role. We also notice that R_{ew} in case d is not equal to zero. Because there is no longitudinal variation in neutral parameters and the thermospheric winds in case d are equal to zero, the EW differences in case d should be driven by the longitudinal variations of geomagnetic fields. By controlling the direction of the field-aligned plasma pressure gradient, the geomagnetic field modifies the value of the field-aligned plasma pressure gradient and the velocity of the plasma field-aligned diffusion, and drives the EW differences in case d.

Zhao et al. (2013) found that R_{ew} varies with solar flux level, and the maximum R_{ew} value and the magnitude of the minimum R_{ew} both increase with increasing solar activity. Zhao et al. (2013) also notice that the lowest minimum R_{ew} occurs around April, with subminimum around September in low solar flux level. As the solar activity increases, R_{ew} gradually shifts to one minimum around June. We also simulated the solar cycle variations of EW differences in NmF2 for case II. In Fig. 4, the top plots show the seasonal and diurnal variations of ΔNmF2, the bottom plots show the seasonal and diurnal variations of R_{ew}, the left plots show the NmF2 EW differences for low solar activity conditions ($F_{10.7}=70$), and the right plots show that for high solar activity conditions ($F_{10.7}=210$). The solid black lines in Fig. 4 represent the zero contours. As shown in Fig. 4a, b, the magnitude of ΔNmF2 mainly increases with the increase of solar flux level. The magnitude of ΔNmF2 for low solar flux level is mainly smaller than that for high solar activity conditions and for medium solar activity conditions (see Fig. 2c). Hence, the magnitude of ΔNmF2 mainly increases with

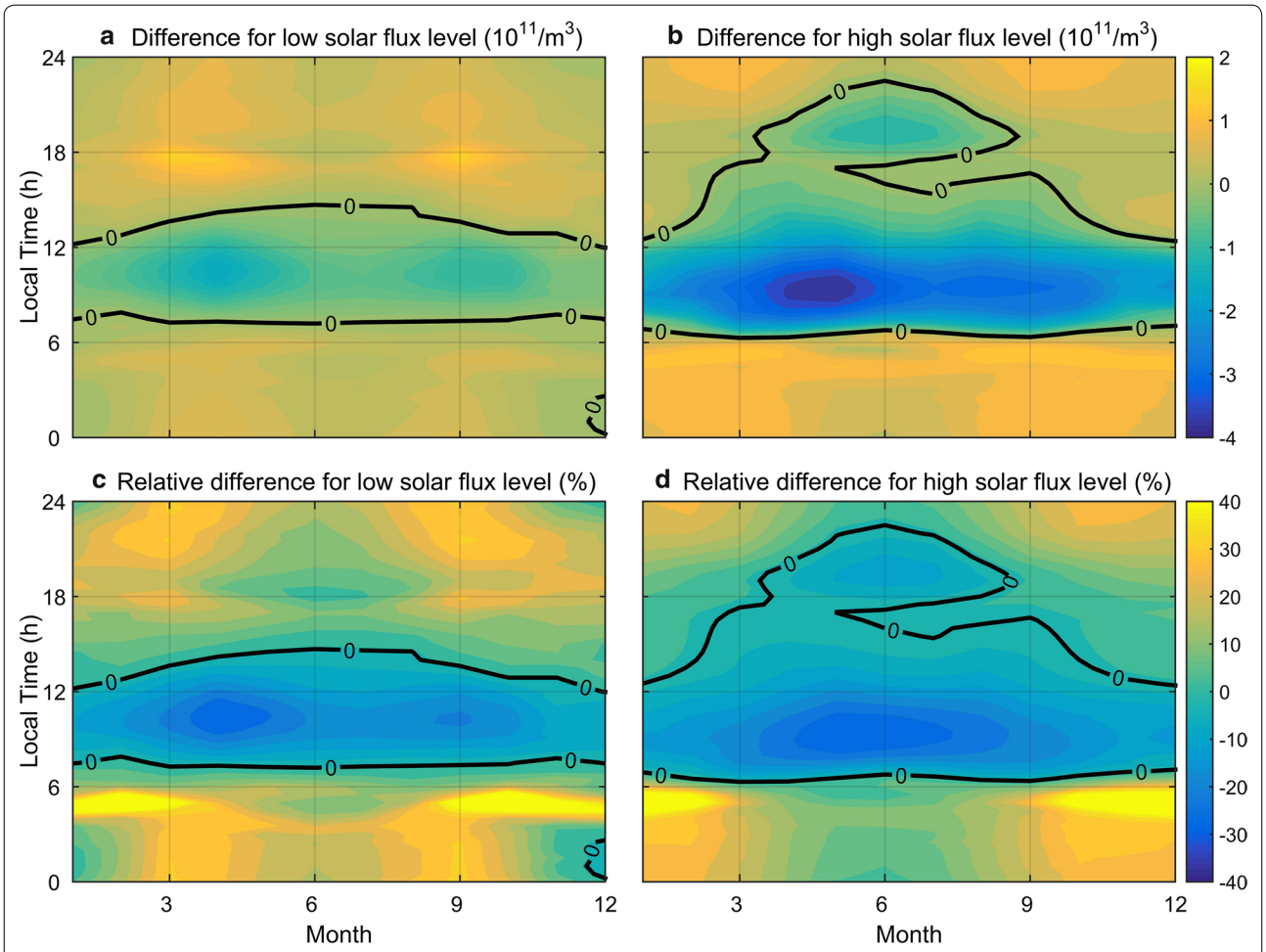

Fig. 4 The solar cycle variations of NmF2 east–west differences. The top and bottom plots, respectively, show the seasonal and diurnal variations of ΔNmF2 (**a**, **b**, in units of $10^{11}/m^3$) and R_{ew} (**c**, **d**, in units of %). The left and right plots, respectively, show the east–west differences for **a**, **c** low and **b**, **d** high solar flux levels. The solid lines in these plots represent the zero lines

the increase of solar flux level. In all solar flux levels, the daytime ΔNmF2 shows two peaks around Spring and around Autumn, and the magnitude of Spring peak is larger than that of Autumn peak. We also notice that there is a negative value area around local summer sunset in high solar flux level, which disappears in low solar activity conditions. The bottom plots of Fig. 4 show the seasonal and diurnal variations of R_{ew}. R_{ew} slightly increases with the increasing of solar flux level. Although R_{ew} for low solar flux level mainly shows obvious semi-annual variations in most of local time, R_{ew} for high solar flux level mainly shows annual variations. Daytime R_{ew} for low solar flux level shows two negative peaks around April and September, and the magnitude of April peak is larger than that of September peak. However, Daytime R_{ew} for high solar flux level only shows a negative peak around June. We should also notice that the daytime R_{ew} for medium solar flux level (Fig. 2d) shows two negative peaks around May and August, and the magnitude of May peak is larger than that of August peak. Hence, we can see two negative R_{ew} peaks around the two equinoxes gradually shift to one negative peak around June Solstice with the increasing of solar flux level. The solar cycle variation of the simulated R_{ew} agrees well with that observed by Zhao et al. (2013).

To analyze the reason for the solar activity dependencies, we simulate ionospheric seasonal and diurnal variations only with zonal/meridional winds for different solar flux levels, and show the simulated results in Fig. 5. In Fig. 5, the top plots show the seasonal and diurnal variations of R_{ew} driven by zonal winds, the bottom plots show that driven by meridional winds, the left plots show the R_{ew} for low solar activity conditions ($F_{10.7}=70$), and the right plots show that for high solar activity conditions ($F_{10.7}=210$). As shown in the top plots of Fig. 5, as the solar activity increases, the two minimum of daytime R_{ew}

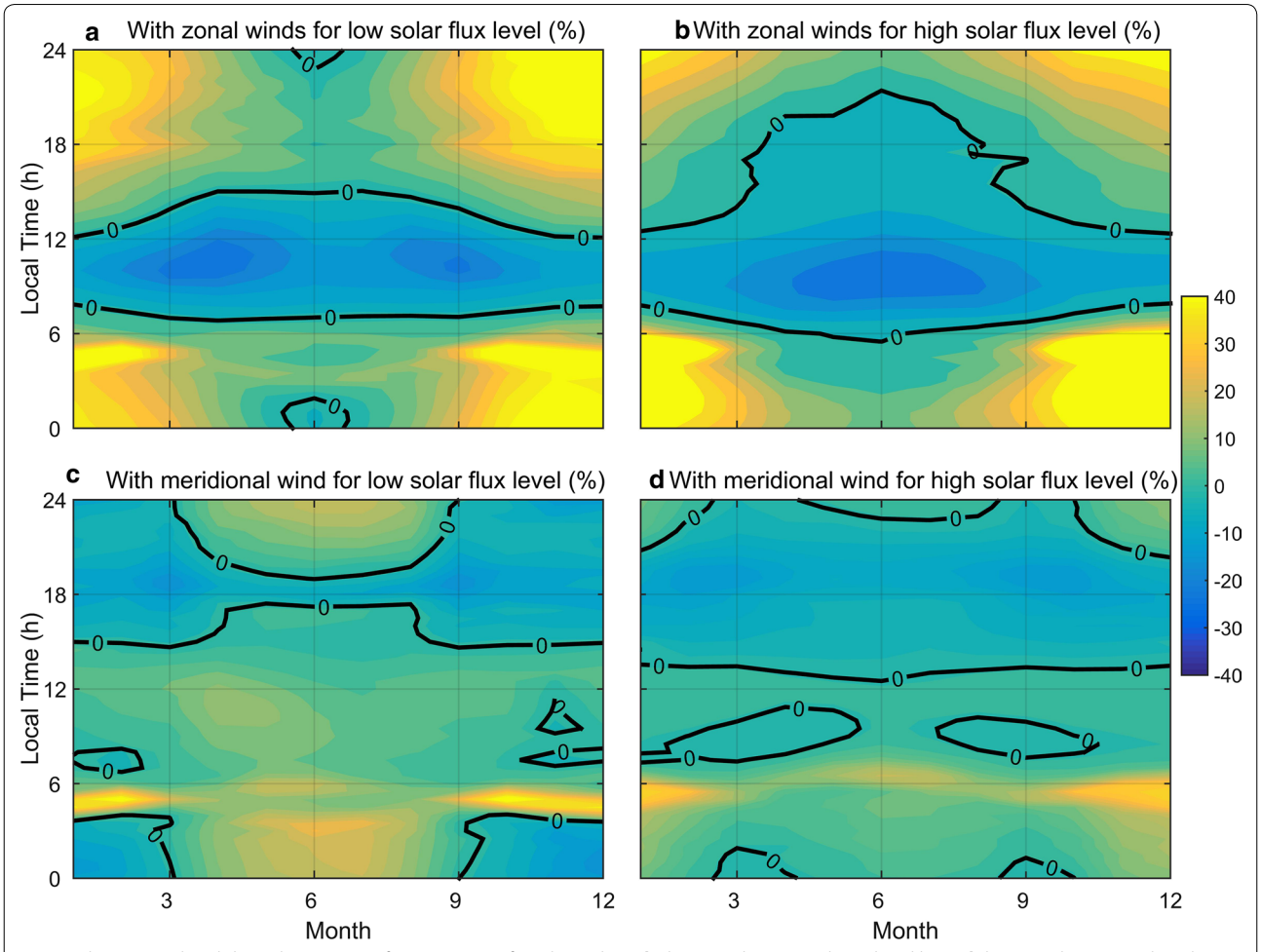

Fig. 5 The seasonal and diurnal variations of R_{ew} (in units of %) driven by **a**, **b** thermospheric zonal wind and by **c**, **d** thermospheric meridional wind. The left and right plots, respectively, show the east–west differences for **a**, **c** low and **b**, **d** high solar flux levels. The solid lines in these plots represent the zero lines

in low solar flux level gradually shifts to one minimum in high solar flux level. However, unlike the zonal winds, the meridional winds drive two new daytime peak values in high solar flux level. Hence, the shift of R_{ew}'s peak with the increase of solar flux level is mainly driven by the zonal winds, whose magnitude and variation patterns can been obtained from HWM93 model (Hedin et al. 1996).

The ionospheric EW difference may also vary with geomagnetic/geographic latitude. Hence, we show the NmF2 EW differences in case II for medium solar flux level at 50° N geographic latitude and at 40°N geographic latitude. In Fig. 6, the top plots show the seasonal and diurnal variations of ΔNmF2 for 50° N (left) and 40° N (right). The black solid lines in Fig. 6 represent the zero contours. As shown in Fig. 6a, b, the ΔNmF2 becomes positive with the decreasing of geographical latitude. The night positive ΔNmF2 at 50° N is smaller than that at 40° N, and the absolute magnitude of daytime negative ΔNmF2 at 50° N is larger than that at 40° N. Although the daytime ΔNmF2 both show two negative peaks around the two equinoxes at 50° N and at 40° N with the Spring peak being larger than the Autumn one, these two peaks gradually shift to June Solstice with the decreasing of geographical latitude. As shown in Fig. 6c, d, similar features can also be found in R_{ew}. The absolute magnitude of daytime negative R_{ew} at 50° N is mainly larger than that at 40° N, and two daytime negative peaks slightly shift to June Solstice with the decreasing of geographical latitude. However, although the night positive R_{ew} at 50° N is still larger than that at 40° N, the difference is weaker than that of ΔNmF2.

To analyze the reason for the latitudinal dependencies, we simulate ionospheric seasonal and diurnal variations only with zonal/meridional wind for different latitudes, and show the simulated results in Fig. 7. In Fig. 7, the top plots show the seasonal and diurnal variations of R_{ew} driven by zonal winds, the bottom plots show that driven

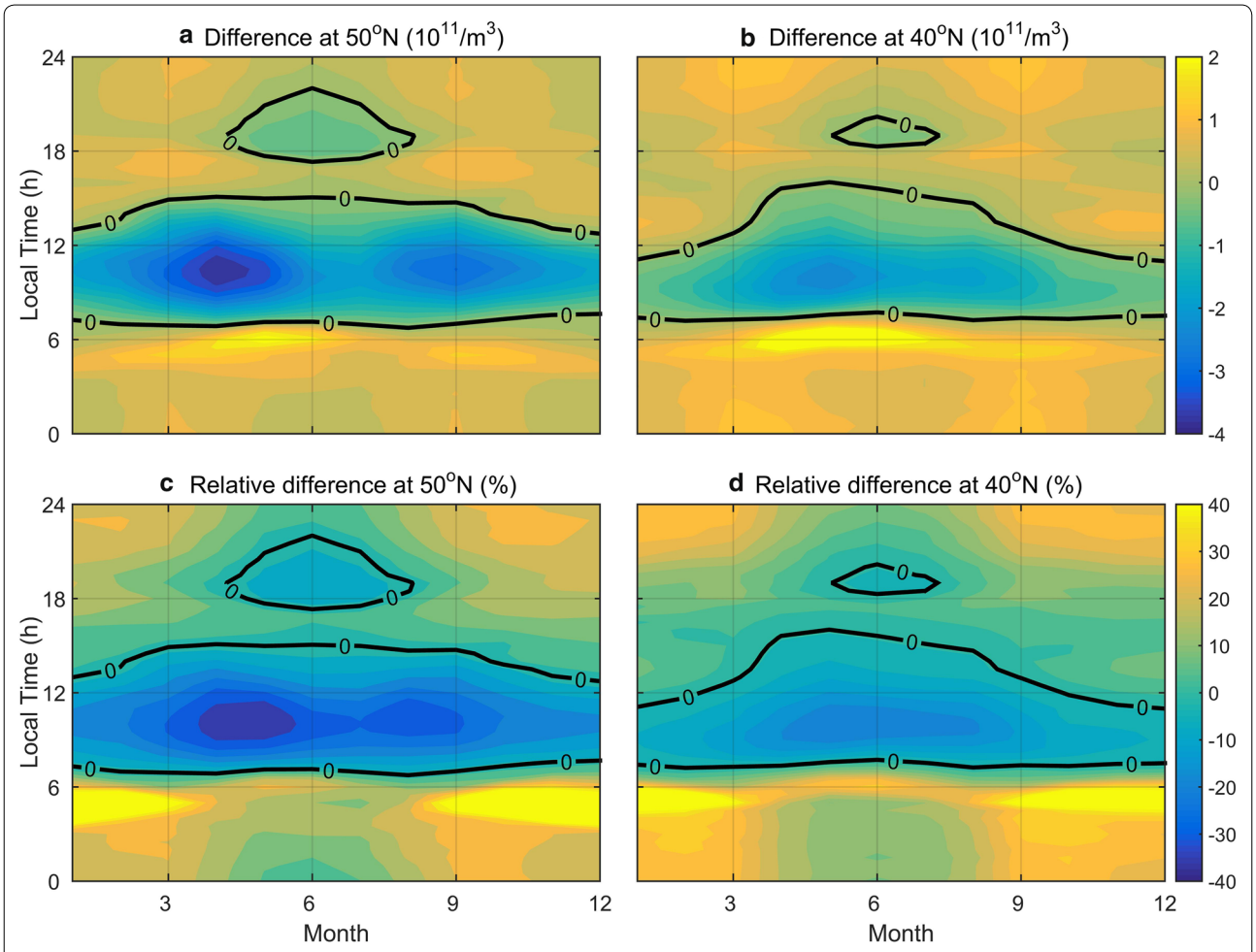

Fig. 6 The latitude variations of NmF2 east–west differences. The top and bottom plots, respectively, show the seasonal and diurnal variations of ΔNmF2 (**a**, **b**, in units of $10^{11}/m^3$) and R_{ew} (**c**, **d**, in units of %). The left and right plots, respectively, show the east–west differences (**a**, **c**) at 50° N and (**b**, **d**) at 40° N. The solid lines in these plots represent the zero lines

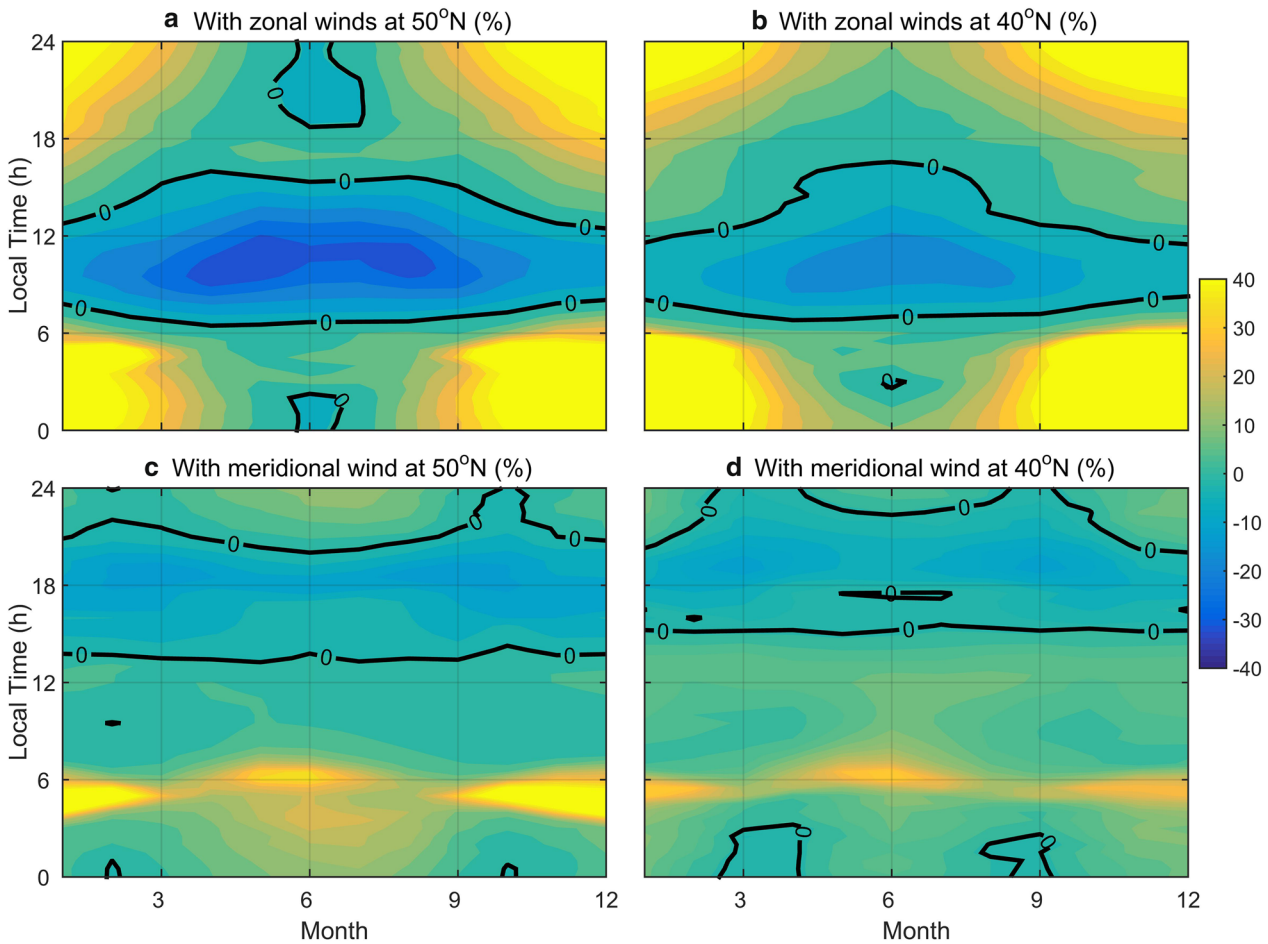

Fig. 7 The seasonal and diurnal variations of R_{ew} (in units of %) driven by **a**, **b** thermospheric zonal wind and by **c**, **d** thermospheric meridional wind. The left and right plots, respectively, show the east–west differences **a**, **c** at 50° N and **b**, **d** at 40° N. The solid lines in these plots represent the zero lines

by meridional winds, the left and right plots, respectively, show the R_{ew} at 50° N and 40° N. As shown in Fig. 7, the absolute magnitude of daytime negative R_{ew} driven by zonal winds at 50° N is mainly larger than that at 40° N. With the decrease of latitude, the daytime negative R_{ew} driven by meridional winds becomes positive. Hence, the latitudinal dependencies of R_{ew} are mainly driven by the zonal winds, and the meridional winds also play a secondary role.

Summary and conclusion

Using TIME3D-IGGCAS model, we simulate the EW differences in NmF2 in the Far East mid-latitude region near the longitudinal sectors with very clear zonal variations of geomagnetic declination, and mainly analyze the influence of the geomagnetic field configuration on the east–west differences. We found that, after removing the longitudinal variations of neutral parameters, TIME3D-IGGCAS can better represent the observed relative east–west (EW) difference (R_{ew}) features. R_{ew}, defined as $R_{ew} = (\mathrm{NmF2_{east}} - \mathrm{NmF2_{west}})/(\mathrm{NmF2_{east}} + \mathrm{NmF2_{west}}) \times 200\%$, is mainly negative (West NmF2 > East NmF2) at noon and positive (East NmF2 > West NmF2) at evening–night. The magnitude of daytime negative R_{ew} is weaker in winter and stronger in summer, and the daytime R_{ew} shows two negative peaks around the two equinoxes. With the increase of the solar flux level, the magnitude of R_{ew} mainly becomes larger, and two daytime negative peaks slightly shift to June Solstice. With the decrease of geographical latitude, R_{ew} mainly becomes positive, and the two daytime negative peaks slightly shift to June Solstice. Through simulations, we have proved that the coupling between the geomagnetic field configuration and thermospheric zonal wind plays a pivotal role in the formation of the ionospheric EW differences in the Far East mid-latitude region. The observed

solar activity dependency of the ionospheric EW differences may be driven primarily by corresponding zonal winds changes with solar activity, whereas the observed latitudinal dependency of the differences is associated with primarily zonal wind and secondarily meridional wind latitudinal variations.

Abbreviations

WSA: Weddell Sea Anomaly; MSNA: Mid-latitude Summer Nighttime Anomaly; EW: East–west; TIME3D-IGGCAS: Three-Dimensional Theoretical Ionospheric Model of the Earth at Institute of Geology and Geophysics, Chinese Academy of Sciences.

Acknowledgements

This work is supported by the Strategic Priority Research Program of Chinese Academy of Sciences (Grant No. XDA17010201), National Science Foundation of China (41674158, 41874179, 41621063, 41674148, 41427901, 41474133, 41322030) and the Opening Funding of Chinese Academy of Sciences dedicated for the Chinese Meridian Project.

Authors' contributions

ZR initiated the study and prepared the manuscript. BZ, WW and LL gave the suggestions and scope of the manuscript and also involved in the discussions and preparation of the manuscript. XL and TY involved in the revision of the paper. All authors read and approved the final manuscript.

Funding

This work is supported by the Strategic Priority Research Program of Chinese Academy of Sciences (Grant No. XDA17010201), National Science Foundation of China (41674158, 41874179, 41621063, 41674148, 41427901, 41474133, 41322030), and the Opening Funding of Chinese Academy of Sciences dedicated for the Chinese Meridian Project.

Availability of data and materials

All the data used in this study are archived in Key Laboratory of Earth and Planetary Physics, Institute of Geology and Geophysics, Chinese Academy of Sciences, and are available on request.

Ethics approval and consent to participate

Not applicable.

Consent for publication

The manuscript does not contain any individual person's data. Not applicable.

Competing interests

The authors declare that they have no competing interests.

Author details

[1] Key Laboratory of Earth and Planetary Physics, Institute of Geology and Geophysics, Chinese Academy of Sciences, Beijing 100029, People's Republic of China. [2] Innovation Academy for Earth Science, Chinese Academy of Sciences, Beijing 100049, People's Republic of China. [3] Beijing National Observatory of Space Environment, Institute of Geology and Geophysics, Chinese Academy of Sciences, Beijing 100029, People's Republic of China. [4] College of Earth and Planetary Sciences, University of the Chinese Academy of Sciences, Beijing 100049, People's Republic of China. [5] School of Space and Environment, Beihang University, Beijing 100083, People's Republic of China. [6] Key Laboratory of Space Environment Monitoring and Information Processing, Ministry of Industry and Information Technology, Beijing 100029, People's Republic of China.

Received: 6 July 2019 Accepted: 4 April 2020
Published online: 15 April 2020

References

Bellchambers WH, Piggott WR (1958) Ionospheric measurements made at Halley Bay. Nature 182:1596–1597. https://doi.org/10.1038/1821596a0

Chang LC, Liu H, Miyoshi Y, Chen C-H, Chang F-Y, Lin C-H, Liu J-Y, Sun Y-Y (2015) Structure and origins of the Weddell Sea Anomaly from tidal and planetary wave signatures in FORMOSAT-3/COSMIC observations and GAIA GCM simulations. J Geophys Res Space Phys 120:1325–1340. https://doi.org/10.1002/2014JA020752

Chen CH, Huba JD, Saito A, Lin CH, Liu JY (2011) Theoretical study of the ionospheric Weddell Sea Anomaly using SAMI2. J Geophys Res 116:A04305. https://doi.org/10.1029/2010JA015573

Chen Y, Liu L, Le H, Wan W, Zhang H (2016) The global distribution of the dusk-to-nighttime enhancement of summer NmF2 at solar minimum. J Geophys Res Space Phys 121:7914–7922. https://doi.org/10.1002/2016JA022670

Dudeney JR, Piggot WR (1978) Antarctic ionospheric research. In: Lanzerotti LJ, Park CG (eds) Upper atmosphere research in Antarctica, Ant. Res. Ser. AGU, Washington, D. C., pp 200–235

He M, Liu L, Wan W, Ning B, Zhao B, Wen J, Yue X, Le H (2009) A study of the Weddell Sea Anomaly observed by FORMOSAT–3/COSMIC. J Geophys Res 114:A12309. https://doi.org/10.1029/2009JA014175

Hedin A, Fleming E, Manson A, Schmidlin F, Avery S, Clark R, Franke S, Fraser G, Tsuda T, Vial F, Vincent R (1996) Empirical wind model for the upper, middle and lower atmosphere. J Atmos Terr Phys 58(13):1421–1447. https://doi.org/10.1016/0021-9169(95)00122-0

Horvath I, Essex EA (2003) The Weddell Sea Anomaly observed with the Topex satellite data. J Atmos Sol Terr Phys 65(6):693–706

Klimenko MV, Klimenko VV, Karpachev AT (2015) Spatial features of Weddell Sea and Yakutsk Anomalies in foF2 diurnal variations during high solar activity periods: interkosmos-19 satellite and ground-based ionosonde observations, IRI reproduction and GSM TIP model simulation. Adv Space Res 55:2020–2032. https://doi.org/10.1016/j.asr.2014.12.032

Kohl H, King JW (1967) Atmospheric winds between 100 and 700 km and their effects on the ionosphere. J Atmos Terr Phys 29:1045–1062

Lean JL, Meier RR, Picone JM, Sassi F, Emmert JT, Richards PG (2016) Ionospheric total electron content: spatial patterns of variability. J Geophys Res Space Phys 121:10367–10402. https://doi.org/10.1002/2016JA023210

Lin CH, Liu JY, Cheng CZ, Chen CH, Liu CH, Wang W, Burns AG, Lei J (2009) Three-dimensional ionospheric electron density structure of the Weddell Sea Anomaly. J Geophys Res 114:A02312. https://doi.org/10.1029/2008JA013455

Liu L, Luan X, Wan W, Ning B, Lei J (2003) A new approach to the derivation of dynamic information from ionosonde measurements. Ann Geophys 21(11):2185–2191

Liu H, Thampi SV, Yamamoto M (2010) Phase reversal of the diurnal cycle in the midlatitude ionosphere. J Geophys Res 115:A01305. https://doi.org/10.1029/2009JA014689

Penndorf R (1965) The average ionospheric conditions over the Antarctic. In: Waynick AH (ed) Geomagnetism and aeronomy, Ant. Res. Ser., vol 4. AGU, Washington, D. C, pp 1–45

Ren Z, Wan W, Liu L, Zhao B, Wei Y, Yue X, Heelis RA (2008) Longitudinal variations of electron temperature and total ion density in the sunset equatorial topside ionosphere. Geophys Res Lett 35:L05108. https://doi.org/10.1029/2007GL032998

Ren Z, Wan W, Liu L, Heelis RA, Zhao B, Wei Y, Yue X (2009a) Influences of geomagnetic fields on longitudinal variations of vertical plasma drifts in the presunset equatorial topside ionosphere. J Geophys Res 114:A03305. https://doi.org/10.1029/2008JA013675

Ren Z, Wan W, Liu L, Xiong J (2009b) Intra-annual variation of wave number 4 structure of vertical E × B drifts in the equatorial ionosphere seen from ROCSAT-1. J Geophys Res 114:A05308. https://doi.org/10.1029/2009JA014060

Ren Z, Wan W, Xiong J, Liu L (2010) Simulated wave number 4 structure in equatorial F-region vertical plasma drifts. J Geophys Res 115:A05301. https://doi.org/10.1029/2009JA014746

Ren Z, Wan W, Liu L, Chen Y, Le H (2011a) Equinoctial asymmetry of ionospheric vertical plasma drifts and its effect on F-region plasma density. J Geophys Res 116:A02308. https://doi.org/10.1029/2010JA016081

Ren Z, Wan W, Liu L, Xiong J (2011b) Simulated longitudinal variations in the lower thermospheric nitric oxide induced by nonmigrating tides. J Geophys Res 116:A04301. https://doi.org/10.1029/2010JA016131

Ren Z, Wan W, Liu L, Le H (2012a) TIME3D-IGGCAS: a new three-dimension mid- and low-latitude theoretical ionospheric model in realistic geomagnetic fields. J Atmos Sol Terr Phys 80:258–266. https://doi.org/10.1016/j.jastp.2012.02.001

Ren Z, Wan W, Liu L, Le H, He M (2012b) Simulated midlatitude summer nighttime anomaly in realistic geomagnetic fields. J Geophys Res 117:A03323. https://doi.org/10.1029/2011JA017010

Ren Z, Wan W, Liu L, Xiong J (2012c) Simulated longitudinal variations in the E-region plasma density induced by non-migrating tides. J Atmos Sol Terr Phys 90:68–76. https://doi.org/10.1016/j.jastp.2011.12.004

Ren Z, Wan W, Xiong J, Liu L (2012d) Simulated equinoctial asymmetry of the ionospheric vertical plasma drifts. J Geophys Res 117:A01301. https://doi.org/10.1029/2011JA016952

Ren Z, Wan W, Xiong J, Liu L (2014) Influence of DE3 tide on the equinoctial asymmetry of the zonal mean ionospheric electron density. Earth Planets Space 66:117. https://doi.org/10.1186/1880-5981-66-117

Richards PG, Nicolls MJ, St.-Maurice J-P, Goodwin L, Ruohoniemi JM (2014) Investigation of sudden electron density depletions observed in the dusk sector by the Poker Flat, Alaska incoherent scatter radar in summer. J Geophys Res Space Phys 119:10608–10620. https://doi.org/10.1002/2014JA020

Richards PG, Meier RR, Chen S-P, Drob DP, Dandenault P (2017) Investigation of the causes of the longitudinal variation of the electron density in the Weddell Sea Anomaly. J Geophys Res Space Phys 122:6562–6583. https://doi.org/10.1002/2016JA023565

Richards PG, Meier RR, Chen S-P, Dandenault P (2018) Investigation of the causes of the longitudinal and solar cycle variation of the electron density in the Bering Sea and Weddell Sea anomalies. J Geophys Res Space Phys 123:7825–7842. https://doi.org/10.1029/2018JA025413

Richmond AD, Blanc M, Emery BA, Wand RH, Fejer BG, Woodman RF, Anguly SG, Amayenc P, Behnke RA, Calderon C, Evans JV (1980) An empirical model of quiet–day ionospheric electric fields at middle and low latitudes. J Geophys Res 85(A9):4658–4664

Thampi S, Lin CH, Liu H, Yamamoto M (2009) First tomographic observations of the midlatitudes summer night anomaly (MSNA) over Japan. J Geophys Res 114:A10318. https://doi.org/10.1029/2009JA014439

Thampi S, Balan N, Lin C, Liu H, Yamamoto M (2011) Mid-latitude Summer Nighttime Anomaly (MSNA)-observations and model simulations. Ann Geophys 29:157–165

Wan W, Liu L, Pi X, Zhang M-L, Ning B, Xiong J, Ding F (2008) Wavenumber-four patterns of the total electron content over the low latitude ionosphere. Geophys Res Lett 35:L12104. https://doi.org/10.1029/2008GL033755

Wan W, Xiong J, Ren Z, Liu L, Zhang M-L, Ding F, Ning B, Zhao B, Yue X (2010) Correlation between the ionospheric WN4 signature and the upper atmospheric DE3 tide. J Geophys Res 115:A11303. https://doi.org/10.1029/2010JA015527

Wan W, Ren Z, Ding F, Xiong J, Liu L, Ning B, Zhao B, Li G, Zhang M-L (2012) A simulation study for the couplings between DE3 tide and longitudinal WN4 structure in the thermosphere and ionosphere. J Atmos Sol Terr Phys 90:52–60. https://doi.org/10.1016/j.jastp.2012.04.011

Wang H, Ridley AJ, Zhu J (2015) Theoretical study of zonal differences of electron density at midlatitudes with GITM simulation. J Geophys Res Space Phys 120:2951–2966. https://doi.org/10.1002/2014JA020790

Zhang S-R, Foster JC, Coster AJ, Erickson PJ (2011) East-West Coast differences in total electron content over the continental US. Geophys Res Lett 38:L19101. https://doi.org/10.1029/2011GL049116

Zhang S-R, Coster AJ, Holt JM, Foster JC, Erickson PJ (2012a) Ionospheric longitudinal variations at midlatitudes: incoherent Scatter Radar Observation at Millstone Hill. Sci China Technol Sci 55(5):1153–1160. https://doi.org/10.1007/s11431-012-4784-y

Zhang S-R, Foster JC, Holt JM, Erickson PJ, Coster AJ (2012b) Magnetic declination and zonal wind effects on longitudinal differences of ionospheric electron density at midlatitudes. J Geophys Res 117:A08329. https://doi.org/10.1029/2012JA017954

Zhao B, Wang M, Wang Y, Ren Z, Yue X, Zhu J, Wan W, Ning B, Liu J, Xiong B (2013) East-west differences in F-region electron density at midlatitude: evidence from the Far East region. J Geophys Res Space Phys 118:542–553. https://doi.org/10.1029/2012JA018235

Publisher's Note